HYPERstream: A multi-scale framework for streamflow routing in large-scale hydrological models.

Sebastiano Piccolroaz[1], Michele Di Lazzaro[2], Antonio Zarlenga[2], Bruno Majone[1], Alberto Bellin[1], and Aldo Fiori[2]

[1]Department of Civil, Environmental, and Mechanical Engineering, University of Trento, via Mesiano 77, I-38122 Trento, Italy
[2]Department of Engineering, Roma Tre University, Via Vito Volterra 62, I-00146 Rome, Italy

Correspondence to: Sebastiano Piccolroaz (s.piccolroaz@unitn.it)

Abstract. We present HYPERstream, an innovative streamflow routing scheme based on the Width Function Instantaneous Unit Hydrograph (WFIUH) theory, which is specifically designed to facilitate coupling with weather forecasting and climate models. The proposed routing scheme preserves geomorphological dispersion of the river network when dealing with horizontal hydrological fluxes,

5   irrespective of the computational grid size inherited from the overlaying climate model providing the input meteorological forcing. This is achieved by simulating the routing within the river network through suitable transfer functions obtained by applying the WFIUH theory to a chosen level of detail. The underlying principle is similar to the block-effective dispersion employed in groundwater hydrology, with the transfer functions used to represent the effect on streamflow of morphological

10   heterogeneity at scales smaller than the computational grid. Transfer functions are constructed for each grid cell with respect to the nodes of the network where streamflow is simulated, by taking advantage of the detailed morphological information contained in the Digital Elevation Model (DEM) of the zone of interest. These characteristics make HYPERstream well suited for multi-scale applications, ranging from catchment up to continental scale, and to investigate extreme events (e.g.,

15   floods) that require an accurate description of routing through the river network. The routing scheme enjoys parsimony in the adopted parametrization and computational efficiency, leading to a dramatic reduction of the computational effort with respect to full-gridded models at comparable level of accuracy. Additionally, HYPERstream is designed with a simple and flexible modular structure that allows for the selection of any rainfall-runoff model to be coupled with the routing scheme and the

20   choice of different hillslope processes to be represented, and makes the framework particularly suitable to massive parallelization, customization according to the specific user needs and preferences, and continuous development and improvements.

1 Introduction

The increasing pressures on freshwater resources originating from a multitude of complex and inter-
acting factors led in recent years to a growing need of tools able to provide water resources informa-
tion at regional to global scales (see e.g., Archfield et al. (2015) for a commentary). Overall, this fos-
tered new developments in large-scale hydrological models as a component of more comprehensive,
and complex, Earth System Models (ESMs). Manabe (1969) was the first to add a land component
in a climate model. His work prompted the development of a first generation of Global Circulation
Models and a parallel development of Land Surface Models (LSMs) for hydrological applications
(see Haddeland et al. (2011) and Prentice et al. (2015) for a comprehensive review). Land Surface
Models are developed with the intent of providing a realistic and detailed representation of vertical
water, energy and CO_2 fluxes, with the perspective to facilitate coupling with atmospheric models.
On the other hand, Large-scale Hydrological Models (LHMs) have been developed with the perspec-
tive of a realistic representation of water resources and horizontal water transfer (Haddeland et al.,
2011). VIC (Liang et al., 1994), LaD (Milly and Shmakin, 2002), H08 (Hanasaki et al., 2008a, b),
Noah-MP (Niu et al., 2011), WEHY-HCM (Kavvas et al., 2013), and CLM (Oleson et al., 2013), are
examples of LSMs, while MacPDM (Arnell, 1999), WBM (Vörösmarty et al., 1998), WGHM (Döll
et al., 2003), WASMOD-M (Widén-Nilsson et al., 2007), PCR-GLOBWB (Van Beek et al., 2011),
LISFLOOD (van der Knijff et al., 2010)), and mHM (Samaniego et al., 2010) can be classified as
belonging to the category of LHMs. This classification notwithstanding, the boundary between these
two categories is blurred since in their recent developments most of these models are converging to
a comprehensive representation of the terrestrial processes, in an attempt to increase realism, though
this is often achieved at the expense of reliability and robustness (Prentice et al., 2015). However, at
the current stage of development, both category of models suffer from a discretization which is often
too coarse to represent routing in the river network with enough detail to capture geomorphological
dispersion (Rinaldo et al., 1991).

The hydrological component of both categories of models, which for simplicity we indicate here
as LHMs, rely on simplified conceptualizations and empirical upscaling procedures (Nazemi and
Wheater, 2015), when dealing with heterogeneities that characterize hydrological fluxes across a
hierarchy of scales, ranging from the hillslope to the catchment and the continent. In addition, most
of the available hydrological models inherit the grid approach from LSMs, which works fine for
the vertical fluxes, but makes streamflow routing grid dependent. The obvious consequence is the
presence of inaccuracies in the representation of horizontal fluxes, unless a very fine discretization
is used, which however is untenable at large scales also for the currently available high performance
computational resources. Indeed, grid-based LHMs are typically applied with a spatial resolution
ranging from 0.1^o (ca. 11 km) to 0.5^o (ca. 55 km), which has been proven to be insufficient to
capture geomorphological dispersion and travel time distribution at the level of accuracy needed to
model horizontal fluxes. This is particularly significant at intermediate scales, i.e., scales of the order

60 of thousand or tens of thousand km^2 (Gong et al., 2009; Verzano et al., 2012), which are relevant in modeling flood events. The introduction of improved routing schemes to adequately resolve horizontal fluxes with an acceptable computational effort is therefore indicated as one of the priorities in ESMs, and in LHMs as well, (Clark et al., 2015).

Hyper-resolution LHMs relying on global digital drainage networks at fine scales, such as Hy-

65 droSHEDS at 90 m resolution (Lehner et al., 2008), represent a possible strategy to overcome the above limitations and obtain reliable estimates of horizontal fluxes (Wood et al., 2011). However, applying a LHM at a such fine discretization is difficult for the large computational cost associated to it, which becomes unbearable when inversion is applied to infer model parameters from observational data. This burden is currently too high for LHMs adopting explicit hydrodynamic routing through

70 the numerical solution of the mass and momentum conservation equations (i.e., the de Saint-Venant equations), but also for models adopting cell-by-cell routing algorithms based on mass conservation and relationships between river-channel storage and streamflows (Yamazaki et al., 2011; De Paiva et al., 2013). If modeling high flow events is the objective of the analysis a hourly, or smaller, time scale should be adopted, thereby further increasing the computational burden, with respect to the

75 daily or monthly time scale typically adopted in large-scale simulations of water resources.

Mixed schemes in which routing is separated from runoff have also been employed (see e.g., Gong et al., 2009, 2011; Wen et al., 2012; Lehner and Grill, 2013). HydroROUT is a vector-based routing scheme fully integrated with ArcGIS (ESRI, 2011) developed by Lehner and Grill (2013), in which streamflow is obtained by routing to the catchment outlet the surface runoff (as provided by

80 an external runoff simulator to be coupled with the routing scheme) accumulated at the nodes of the network. Routing is performed by using a 'plug-flow' routing scheme similar to that implemented by Whiteaker et al. (2006) and applied to the HydroSHEDS river network (Lehner et al., 2006).

Wen et al. (2012) proposed a multi-scale routing framework employing a pdf distribution for the overland flow path lengths lumping the effect of unmodeled sub-grid variability in the parameters

85 describing the pdf. The kinematic wave routing method is then employed for both overland and channel flow simulations, thereby resulting in a highly computational demand, as already discussed above. In addition, the routing scheme generates streamflow only at the outlet of the catchment without the possibility to simulate streamflows at internal nodes, such as lakes, reservoirs or other infrastructures, while the use of response functions aggregated at the daily time scale limits the

90 applicability to flood events occurring in large river basins, with the approach proposed by Gong et al. (2009, 2011).

To overcome the above limitations without resorting to hyper resolution hydrological models (when not needed to better reproduce spatial variability of soil water storage and transmission), we propose a multi-scale approach for streamflow routing based on the travel time approach. More

95 specifically, we propose a scheme based on the Width-Function Instantaneous Unit Hydrograph (WFIUH) theory (see e.g., Rodríguez-Iturbe and Rinaldo, 1997), applied to a hybrid raster-vector

data structure, according to the definition proposed by Lehner and Grill (2013). The proposed scheme is designed to work at large, up to the continental, spatial scales with the resolution of the computational grid inherited directly from the climate or weather forecasting models used to simulate the input meteorological forcing. Similarly to LHMs water storage and runoff generation processes (we call this part the land component of the model) are simulated according to this relatively coarse grid, whilst streamflow routing is performed through a scheme that is irrespective of this spatial resolution thus allowing for an improved reproduction of horizontal water transfers. Here we refer to as "perfect upscaling" to indicate that the proposed routing scheme keeps the network contribution inherently invariant with respect to the grid size of meteorological forcing, i.e. geomorphological dispersion (Rinaldo et al., 1991) is preserved as it is derived from the morphological information embedded in the available DEM. Scale-invariance is an important feature characterizing our modeling approach not enjoyed by grid-based LHMs, which rely on empirical upscaling procedures in order to represent unmodeled geomorphological dispersion. Here perfect upscaling is presented for the case study of Upper Tiber (central Italy), where we show that our routing scheme does not entail any deterioration in the watershed width functions when considering progressively coarser spatial resolutions. An additional crucial aspect is the computational time efficiency, which stems from the fact that the most demanding step of the procedure is the computation of the geomorphological width functions, which is performed only once as an offline pre-processing procedure. This characteristic, coupled with easiness of parallelization and parsimony in parameterization, inspired us to coin the name HYPERstream, where "HYPER" recalls that the proposed model is based on a HighlY Parallelizable and scalablE Routing scheme. Finally, HYPERstream is designed with a flexible and modular structure which allows the coupling with any lumped or process-based formulation for infiltration and subsurface flow processes, while the simplicity and computational efficiency makes it an appealing tool for uncertainty assessment of the predictions, and in general for simulations conducted in a Monte Carlo framework.

This paper is organized as follows: Section 2 describes the multi-scale hydrological conceptual model, details of the pre-processing module and derivations of node specific width functions are provided in Section 3, with reference to the Upper Tiber case study. An example of application for two flood events is discussed in Section 3.3, and finally concluding remarks are drawn in Section 4.

2 Model development

As stated in the Introduction, our aim is to develop a simple, parsimonious and computationally efficient method for streamflow routing (with particular attention to floods) in large river basins. To this aim, we adopt different modeling strategies for the river network and the associated hillslopes (the land component introduced in Section 1): a linear, geomorphologically-based approach for the former, and a lumped formulation for the latter. We note that the land component can be decided

4

without particular restrictions, depending only on the user's needs and preferences. The proposed modeling framework reflects the current understanding of hydrological processes at the hillslope and watershed scales (see e.g., Sivapalan, 2003).

135   The sketch of Fig. 1 displays the conceptual model adopted here. The modeled domain A, which can be of any size and may include any number of disconnected river networks (for example, the sketch of Fig. 1 contains two river networks), is subdivided into N macrocells, each one characterized by a contributing area $A^{(i)}$, such that $\sum_{i=1}^{N} A^{(i)} = A$. We emphasize that the generic $A^{(i)}$ does not need to coincide with the macrocell area, for instance this happens when the macrocell contains

140   parts of neighbor watersheds (see the macrocells at the boundary of Fig. 1). There are no constraints on A, except that it must cover all the watersheds of interest. For easiness of representation, in Fig. 1 macrocells are represented as squares, but this is not by any means a limitation of the model and irregular macrocells can be used if convenient in the application of the model. Indeed, size and geometry of the macrocells can be set to coincide with the gridding of the weather or climate model

145   used to provide the input meteorological forcing.

The drainage characteristics of the basins are obtained from the DEM of the area of interest. The spatial resolution of the DEM should be fine enough to adequately capture the spatial structure of the drainage basins and the embedded river networks. Following procedures widely adopted for the identification of drainage direction and hillslope-channel separation (Tarboton et al., 1991; Montgomery

150   and Foufoula-Georgiou, 1992) (see Sect. 3.2), the river networks are extracted and the hillslopes identified.

The area of the hillslopes changes through the domain, unless identification of the river networks is performed by using a constant threshold area. The link between the hillslope and the channel is denoted as hillslope-channel transition site. As an example, a synthetic DEM grid is shown in Fig. 1

155   (25 DEM cells per macrocell) together with the identified river network. The figure shows also a few hillslopes (colored areas), each of them associated to the corresponding hillslope-channel transition site (colored squared symbols). Notice that in the example the brown hillslope is divided between two macrocells ($i = 1, 2$), a common situation in our approach since the discretization of the domain into macrocells may be arbitrary (i.e., it does not necessarily use topographic information, as is

160   generally the case in weather forecasting or climate models).

The next step in the construction of the model is the identification of the N_k nodes where streamflow is simulated. In the example of Fig. 1, $N_k = 5$ nodes, identified by red bullets, are distributed within two networks. No limitations are imposed to the number and position of these nodes, which represent locations were streamflow is computed either to compare it with observational data, as part

165   of the inversion procedure, or for other purposes, such as to verify flood protection structures (or the need to build them). Each macrocell i may feed one or more nodes; for instance, the macrocell $i = 3$ in Fig. 1 includes contributing areas to nodes $k = 1$ and $k = 2$, with different routes. It may also occur that a macrocell contributes to the same node k with different routes, as for the case of

5
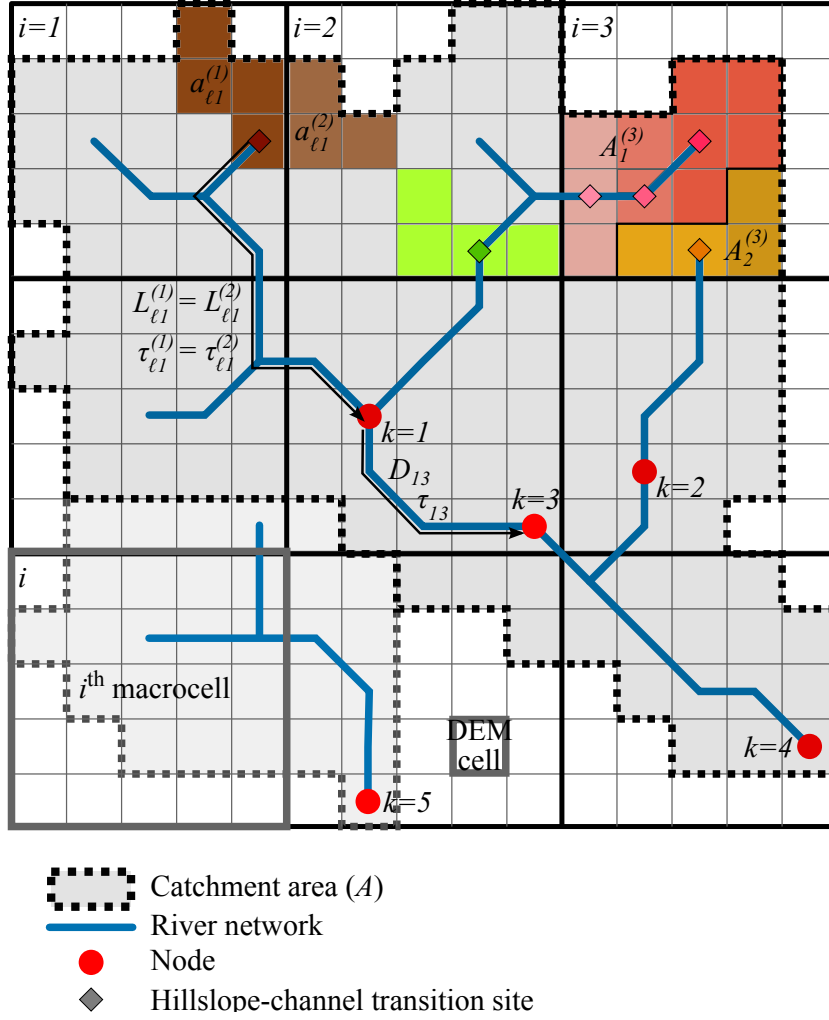
Figure 1. Sketch of basin conceptualization: subdivision of the study area into macrocells and nodes (red dots). River network is subdivided into hillslope-channel transition sites (colored squared symbols) each associated to a pertaining hillslope area $a_{\ell k}^{(i)}$ (colored areas). For this simple case we consider $N = 9$ macrocells and $N_k = 5$ nodes. An example of two pathways characterized by the same length $L_{\ell k}^{(i)}$ and travel time $\tau_{\ell k}^{(i)}$ is also sketched.

macrocell $i = 2$ which contributes to node $k = 1$, through both hillslopes highlighted in green and

170   brown.

We denote with $A_k^{(i)}$ the area of macrocell i contributing to node k, such that $\sum_{k=1}^{N_k} A_k^{(i)} = A^{(i)}$. Notice that $A_k^{(i)} = 0$ if the macrocell i does not contribute to node k. The runoff generation processes occurring at the hillslope scale can be modeled by using schemes of different level of complexity, from the simple SCS-CN method (U.S. Soil Conservation Service, 1964) to methods based on the

175   solution of the Richards equation, or one of its simplification (Clark et al., 2015), depending on the objectives of the analysis. Whatever the hillslope model, for the sake of generality hereafter we indicate with $\eta_{\ell k}^{(i)}$ $[L/T]$ the water discharge per unit area produced by the hillslope ℓ of area $a_{\ell k}^{(i)}$

$[L^2]$, which belongs to the macrocell i and contributes to the streamflow at the closest downstream node k along the river network (for instance, the hillslope highlighted in green in Fig. 1 contributes to node $k = 1$, which is the first node encountered moving downstream). The resulting water flow is triggered by rainfall or snowmelt and depends on the partitioning of hydrological fluxes at the hillslope scale, according to the selected hillslope model and the hydrological processes that are simulated. According to the above conceptual scheme, water flow produced by the hillslope enters the network system through the hillslope-channel transition site, and is subsequently routed through it.

From this kinematic scheme, it follows that the streamflow contribution of the hillslope ℓ, belonging to the macrocell i, to node k can be written as follows

$$q_{\ell k}^{(i)}(t) = A_k^{(i)} \tilde{a}_{\ell k}^{(i)} \int_0^t \eta_{\ell k}^{(i)}(t-\tau)\, \delta\left[\tau - \tau_{lk}^{(i)}\right] d\tau = A_k^{(i)} \tilde{a}_{\ell k}^{(i)} \eta_{\ell k}^{(i)}(t - \tau_{\ell k}^{(i)}), \tag{1}$$

where $\tilde{a}_{\ell k}^{(i)} = a_{\ell k}^{(i)}/A_k^{(i)}$ $[-]$ is the relative hillslope area, δ $[1/T]$ is the Dirac delta function, $\tau_{\ell k}^{(i)}$ $[T]$ is the travel time from the hillslope-channel transition site of the hillslope ℓ to node k, and t $[T]$ is the current time.

Under the hypothesis that the stream velocity V_c $[L/T]$ is constant through the network, the travel time assumes the following expression: $\tau_{\ell k}^{(i)} = L_{\ell k}^{(i)}/V_c$, where $L_{\ell k}^{(i)}$ is the distance, measured along the network, from the hillslope-channel transition site of the hillslope ℓ to the first downstream node k. The assumption of constant V_c is crucial for the linearity of the processes at the watershed scale, as stated at the beginning of this section. Eq. (1) is consistent with the general conceptual framework used to derive the Width Function Instantaneous Unitary Hydrograph by rescaling the geomorphological width function through a suitable constant velocity (Gupta et al., 1986; Mesa and Mifflin, 1986; Gupta and Mesa, 1988; Rodríguez-Iturbe and Rinaldo, 1997). We note that the assumption of constant channel velocity is supported by experimental measurements, especially for high flow conditions (see e.g., Pilgrim, 1976, 1977). Additionally, stream hydrodynamic dispersion is neglected, owing to its small to negligible effect on the hydrological response, which has been demonstrated to be dominated by geomorphological dispersion already embedded into the rescaled width function (Rinaldo et al., 1991, 1995; Rodríguez-Iturbe and Rinaldo, 1997).

The streamflow $q_k^{(i)}$ $[L^3/T]$ generated by macrocell i and contributing to the node k is then obtained by summing up all the contributions stemming from the hillslopes of the macrocell draining to the node k:

$$q_k^{(i)}(t) = A_k^{(i)} \sum_\ell \tilde{a}_{\ell k}^{(i)} \int_0^t \eta_{\ell k}^{(i)}(t-\tau)\, \delta\left[\tau - \tau_{lk}^{(i)}\right] d\tau. \tag{2}$$

Under the hypothesis that the hillslope water discharge per unit area is constant through the cell i, i.e. by assuming that $\eta_{\ell k}^{(i)} = \eta^{(i)}$, Eq. (2) simplifies to:

$$q_k^{(i)}(t) = A_k^{(i)} \int_0^t \eta^{(i)}(t-\tau) f_k^{(i)}(\tau) d\tau = A_k^{(i)} \eta^{(i)} * f_k^{(i)}(t), \tag{3}$$

where $f_k^{(i)}(\tau) = \sum_\ell \tilde{a}_{\ell k}^{(i)} \delta \left[\tau - L_{\ell k}^{(i)}/V_c\right]$ is the probability density function (pdf) of the travel time $\tau_{\ell k}^{(i)}$ weighted by the relative hillslope area $\tilde{a}_{\ell k}^{(i)}$. In Eq. (3) the asterisk denotes convolution.

Finally, water discharge $Q_k(t) \left[L^3/T\right]$ at the node k is given by the sum of the direct contribution of each macrocell i to the node plus the contribution of the nodes upstream of k:

$$Q_k(t) = \sum_{i=1}^N q_k^{(i)}(t) + \sum_{i=1}^N \sum_{j=1}^{N_k^{up}} q_j^{(i)}(t - \tau_{jk}), \tag{4}$$

where $\tau_{jk} = D_{jk}/V_c$ is the travel time from the node j, located upstream to the node k, to the node k, D_{jk} is the distance between the two nodes, and N_k^{up} is the number of nodes upstream of k. In the first right hand term of Eq. (4) summations are extended over all the macrocells, with the convention that $q_k^{(i)} = 0$, because $A_k^{(i)} = 0$, for all macrocells not contributing, i.e. not connected through the network, to the node k (the same applies for index j). Notice that, in the second right hand term of (4) the streamflow computed at the node j is rigidly translated to the node k with the delay τ_{jk} depending on the distance between the two nodes, thereby neglecting again the effect of stream hydrodynamic dispersion, as typically done in the WFIUH approach (see e.g., Gupta et al., 1986; Van Der Tak and Bras, 1990; Botter and Rinaldo, 2003; Giannoni et al., 2005).

The above method is simple and computationally effective. The underlying principle is similar to the block-effective dispersion employed in groundwater hydrology (see e.g., Rubin et al., 1999; De Barros and Rubin, 2011), with the travel time pdf used to represent the effect on streamflow of morphological heterogeneity at scales smaller than the macrocell, with a lower cutoff given by the DEM scale. The linearity of the transfer processes at the scale of the network makes the algorithm easy to parallelize, making it promising for large-scale applications at small time scales (i.e., with hourly or sub-hourly time step). In principle, streamflow generated by a macrocell can be elaborated by a single processor (with the convolution of Eq. (3) being the most demanding step), for the whole duration of the simulations, independently from the other processors. Then, the streamflow $Q_k(t)$ at the nodes of interest is further processed with Eq. (4) when all processors terminated the elaboration of their macrocell. For the same reasons, this model is particularly suited to multiple Monte Carlo runs (e.g., for parameter estimation, uncertainty analysis, multi-model or multi-scenario analysis). The main advantage of the method is that, by design, it preserves the global geomorphological dispersion of the basin, as calculated by the fine grid DEM, no matter the size of the macrocells. Consequently, the upscaling of river network dispersion is perfectly resolved, without resorting to hyper-resolution

numerical grids. This point shall be illustrated in the ensuing section. Spatial variability of precipitation, which indeed plays a fundamental role in shaping the hydrological response of river basins at intermediate spatial scale (i.e., beyond a few thousands of km^2, see Nicótina et al. 2008; Volpi et al. 2012; Sapriza-Azuri et al. 2015), is in our scheme inherited from the companion climatic model and it is embedded in the hillslope production function η according to the macrocell resolution. Similar approaches relying on distributed versions of geomorphological response, but generally based on a partition of the watershed into natural or anthropogenic sub-basins and not focused on large scales applications, can be found in Naden (1992), Moussa (1997), Rinaldo et al. (2006), Hallema et al. (2013),Hallema and Moussa (2014), Rigon et al. (2015), and Bellin et al. (2016).

Routing requires the definition of only a parameter, the channel velocity V_c, which is a very parsimonious, yet effective, parametrization with respect to grid-based routing schemes. If the DEM resolution is high and the total domain A where the model is applied is large, the preprocessing step can be time consuming; the effort is however compensated in the application of the model, particularly if the modeling activity is performed in a multiple run framework. We note that the only pre-processing operation required is the analysis of the DEM aimed at identifying the river network and the drainage characteristics of the river basin, and at computing the geomorphological width functions.

3   Description of the model features, with application to the Upper Tiber Basin

3.1   Study area

In this section we describe an application of HYPERstream to the Upper Tiber river basin, providing a practical example of model characteristics and performances. The study area covers the upper portion of the Tiber river basin, located along the Apennine ridge (central Italy) between $42^o\,36'$ and $43^o\,51'$ latitude North and $11^o\,48'$ and $12^o\,55'\,12''$ longitude East (see Fig. 2a). The basin drains an area of approximately $4000\,km^2$ which represents about 25% of the entire Tiber basin at the river mouth in the Tyrrhenian sea. The basin is predominantly mountainous, with elevation ranging from 145 to $1560\,m\,a.s.l.$ (see Fig 2b) and it is aligned to the North-West South-East direction, with the Apennine ridge-line representing an important physical boundary at East that causes variability in precipitation and temperature. From a geological point of view most of the catchment is underlined by low-permeability formations, chiefly flysch, sandstone clay, and limestone clay. However, high-permeability formations (calcareous lithology) are found in the upper part of the basin and on the eastern divide.

Intense precipitation events are typically associated with humid frontal advection from the Mediterranean sea and condensation due to the orographic uplift. Because of strong topographic gradients, headwaters experience intense rainfall events, mostly occurring from autumn to spring, associated with frequent flood events. Substantial flood events have been also observed in the floodplain of the
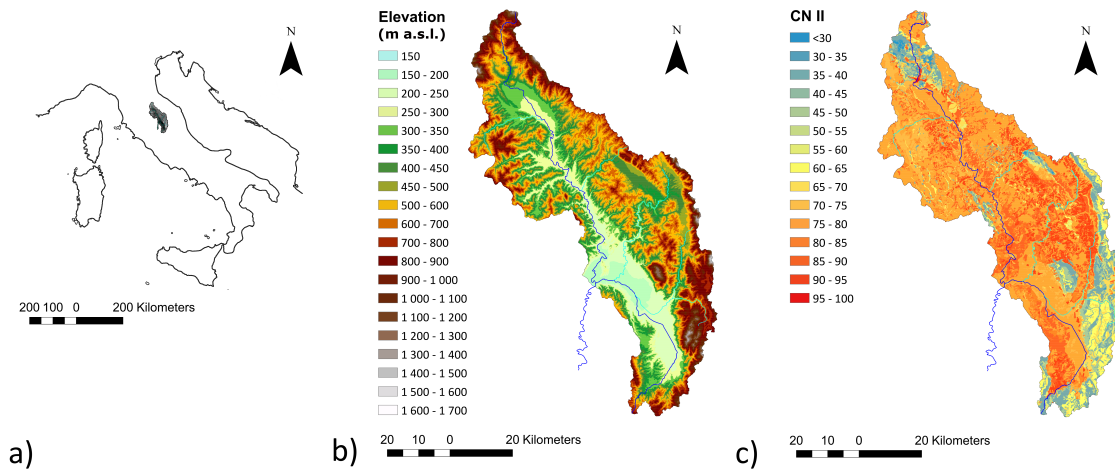
Figure 2. Maps showing: a) the location of the Upper Tiber river basin within the Italian Peninsula, b) DEM of the watershed and c) fine scale land classification according to the CN II parameter.

river (southern part) where most of population and economical activities are clustered (Manfreda et al., 2014). Topography is represented through a $20\,m$ resolution DEM provided by the Istituto Geografico Militare (IGM, available online at http://www.igmi.org/). Digital maps of land use and lithological characterization were supplied by the European Environmental Agency (Corine Land

280　Cover project) and by Italian Agency for Environmental Protection and Research (ISPRA), respectively (maps not shown). Furthermore, land use classes from Corine classification and infiltration capacity estimates were used to associate at each DEM cell a value of the Curve Number parameter (CNII, see Fig. 2c), which shall be used in the SCS-CN runoff model as described in Sect. 3.3.

3.2　Macrocell discretization, width functions derivation and perfect upscaling

285　The control sections adopted for multi-site model validation (see Sect. 3.3) are located at 5 stream-gauge stations: Santa Lucia (SL), Ponte Felcino (PF), Ponte Bettona (PB), Ponte Rosciano (PR) and Ponte Nuovo (PN), with the latter being the outlet of the river basin (see Fig. 3). Drainage area (ranging between 1000 and $4000\,\mathrm{km}^2$), longest flow path, and other geomorphic characteristics of the sub-catchments identified by the 5 control nodes are reported in Table 1. The control nodes are located

290　along the main course of the Tiber river and its two major tributaries (Chiascio and Topino rivers), and they are equipped with gauges registering water levels at 30 minutes time step. Stage measurements in the period 1990-2000 together with validated stage-discharge relationships have been provided by the Hydrographic Service of Umbria Region (http://www.idrografico.regione.umbria.it). The meteorological forcing is described with half-hourly precipitation at 32 meteorological stations

295　managed by the same institution. Fig. 3 shows a map with the locations of the meteorological and stream gauging stations together with the subdivision of the watershed into the 5 inter-basin areas.

10
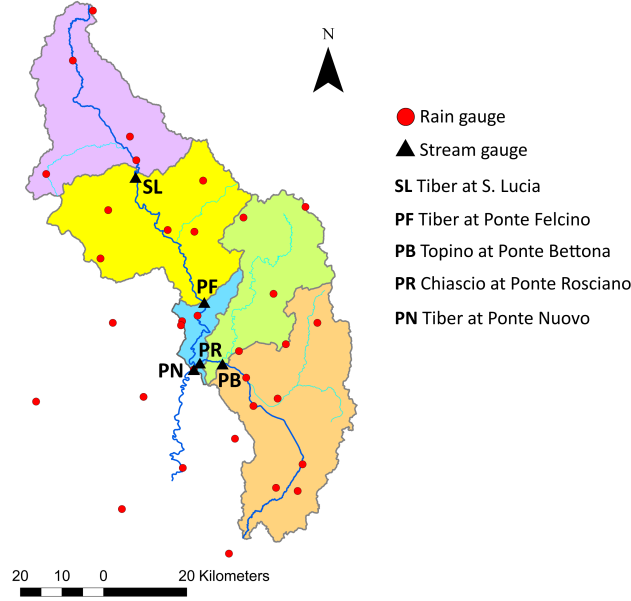
Figure 3. Map showing the subdivision of the watershed into 5 inter-basins, each one identified by a node where water discharge is computed (black triangles). The location of the meteorological stations are also shown as colored dots.

In the following the effect of spatial discretization on the hydrologic response is analyzed with reference to macrocells of different dimensions. In particular, the study area was overlaid with macrocells of increasing size, from 1 to 150 km (the latter including the whole Upper Tiber river basin within a single macrocell), and corresponding to about $37''$ and $1^o 36'$, respectively. Domain discretization with macrocells of 5, 10 and 50 km are shown as an example in Fig. 4.

The identification of the drainage network and associated geomorphic metrics was performed by adopting standard DEM pre-processing techniques. In particular, the identification of the flow path lengths involved the following steps: (i) pit and flat area removal following the procedure of Tarboton et al. (1991); (ii) determination of the drainage directions by using the standard single direction D8 algorithm (O'Callaghan and Mark, 1984); (iii) calculation of the space filling tree network, which connects each site to the outlet; (iv) definition of channel initiation, by adopting a combination of the threshold-slope area and the threshold-support area criteria (Di Lazzaro, 2009).

For a given resolution of the macrocell grid, it is thus possible to derive the frequency distribution $f_k^{(i)}$ of the flow path lengths $L_{\ell k}^{(i)}$ pertaining to macrocell i and connecting the hillslope-channel transition site of the hillslope ℓ to the control node k (i.e., the macrocell-node specific width functions introduced in Section 2), which is the best possible approximation of the width function, given the scale of the DEM.

Fig. 4 shows as an example width functions constructed at the Santa Lucia node (upstream node on the main river-course, see Fig. 3), for a few macrocells of size 5 km, 10 km, and 50 km, respectively.

11

When the macrocell is small with respect to the sub-catchment, its width function is narrow, since it includes a reduced number of hillslopes. Conversely, when the macrocell is large enough to cover the entire sub-catchment, its width function tends towards that of the sub-catchment. The first case is approached by the discretization with macrocells of 5 km (left panels in Fig. 4). The width functions of three selected macrocells, identified with different colors, are all narrow and centered around a varying median value. On the other hand, when the size of the macrocell grows to 50 km (right panels in Fig. 4), most of the hillslopes are contained into the macrocell colored in yellow, whose width function is close to that of the entire sub-catchment (see the grey line in the bottom panel). The intermediate 10 km discretization produces consistent results, showing wider width functions, with less variable median values with respect to the 5 km discretization. This is consistent with the underlying rationale of the model, which is intended to keep the geomorphologic component of dispersion as it is derived from the finest scale description of topography at hand (i.e., the DEM scale), even when runoff generation processes are represented at a larger scale (e.g., to comply with the output of climate models). When all the width functions of the macrocells contributing to the SL node are combined (i.e., 57, 19 and 2 macrocells for 5, 10 and 50 km, respectively), the global width functions are exactly the same for the three discretizations (compare the three graphics in the lower panel of Fig. 4), thereby confirming that routing is insensitive to the size of the macrocell, as desired. Hence, upscaling of geomorphological dispersion is by construction free of errors or scale effects, in our approach. This is not the case for models in which the geomorphological description of the drainage network is performed at the same scale of the macrocells grid (see the discussion in the Introduction). To show this, in Fig. 5 we compare the width function calculated at Ponte Nuovo, the outlet of the catchment, derived from the original 20 m DEM (grey line), which in our formulation is perfectly preserved for any choice of the macrocell size, with the corresponding width functions obtained after DEM aggregation at 5 km (blue), 10 km (orange), and 50 km (red), respectively. The figure shows, in particular, how aggregating digital topographic information over areas of progressively increasing size (as inevitably occurs when routing is performed by using any cell-based scheme) results in a deterioration of the width function, and, as a consequence, of the geomorphologic response of the watershed. This is not the case in our formulation in which the width function preserves the information derived from the spatial resolution of the DEM, irrespective of the resolution of the adopted runoff generation model.

3.3 Application example

In this section we present an example of application of HYPERstream for flood prediction in the Upper Tiber basin, with the purpose to illustrate its major computational and functional features. To focus on the routing scheme, the exercise has been intentionally kept as simple as possible. In particular, the hillslope production function has been defined by combining the widely used SCS-CN method (U.S. Soil Conservation Service, 1964) for runoff simulation with a linear reservoir model

12
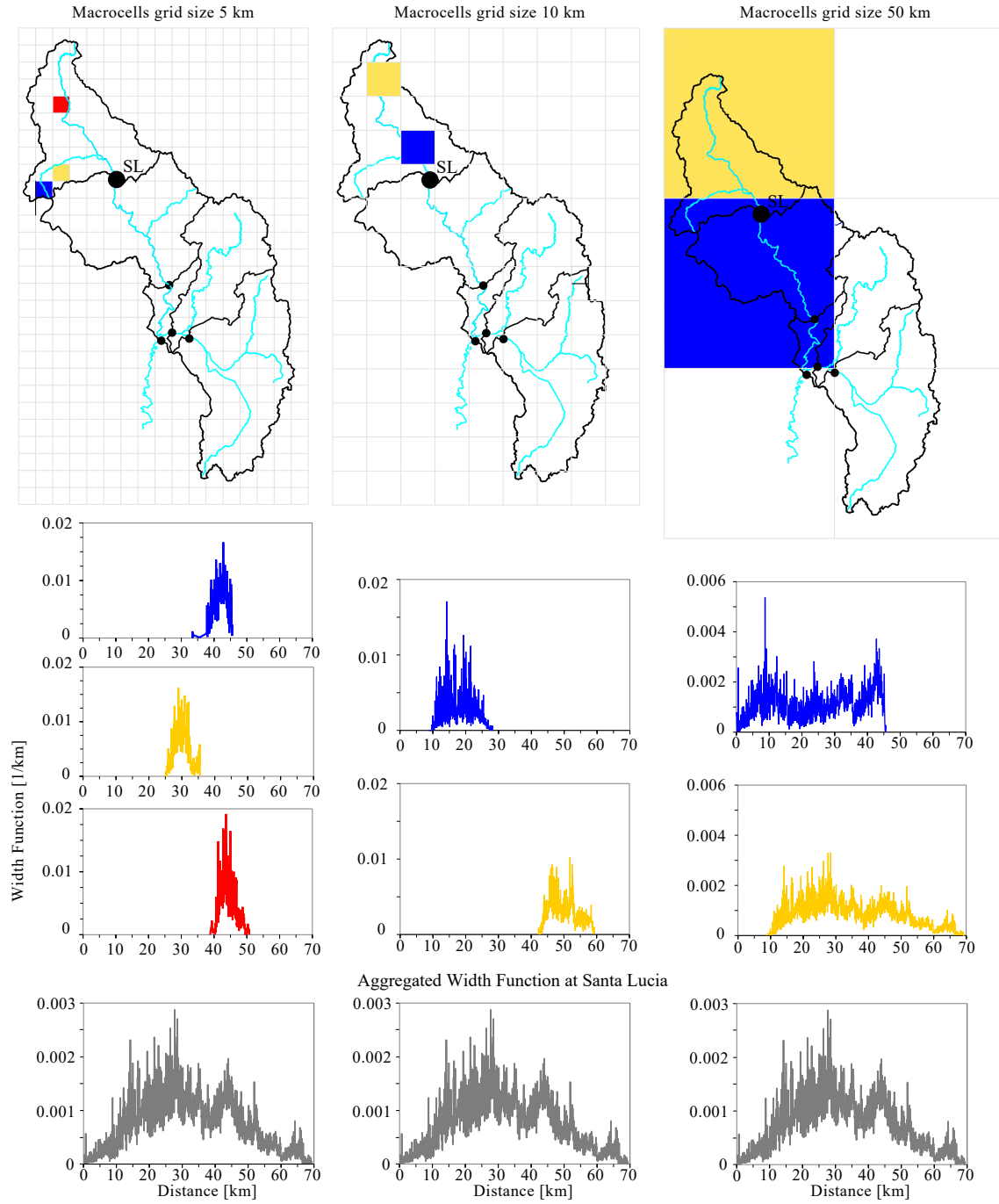
Figure 4. Width functions computed at the Santa Lucia (SL) control section for selected macrocells (colored lines) and for the whole sub-catchment (grey lines, panels at the bottom), considering grid sizes of 5 km, 10 km and 50 km. The width function of the whole sub-catchment is by design the same for the three spatial resolutions.
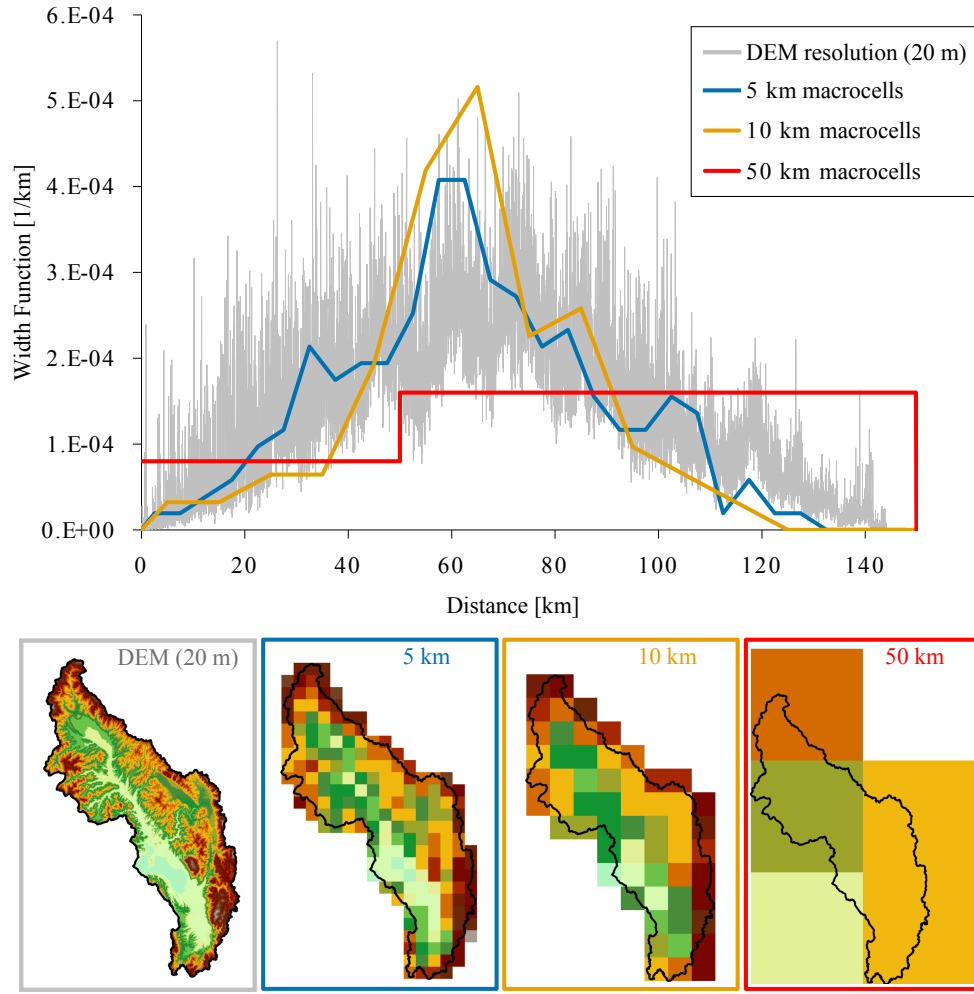
Figure 5. Width functions of the Upper Tiber river basin at Ponte Nuovo (PN) outlet (4116 km^2) obtained aggregating the original 20 m DEM to 5 (blue), 10 (orange), and 50 (red) km. The width function derived from the original 20 m DEM is also shown (grey). Aggregated DEMs with grid size of 5, 10, and 50 km are shown in the lower part of the figure.

describing the travel time distribution within the hillslope (Rodríguez-Iturbe and Rinaldo, 1997, ch. 7.3). This is consistent with the notion that travel times in hillslopes are important in shaping the hydrologic response of a watershed and cannot be neglected even for large river basins, where the channeled lengths are usually much larger than the mean hillslope size (Botter and Rinaldo, 2003; D'Odorico and Rigon, 2003; Di Lazzaro and Volpi, 2011). Subsurface contribution to streamflow was not explicitly considered for this specific model configuration, which is focused on floods. As a possible alternative to the linear reservoir model, a rescaled hillslope width function could be used to represent the travel time distribution at the hillslope scale. In this case, rescaling may be obtained by using a hillslope specific velocity $V_\ell << V_c$.

14

At the hillslope scale runoff is computed by using the classic SCS-CN scheme:

$$R_i(t) = \frac{(P_i(t) - I_{a,i})^2}{P_i(t) + c_S S_i - I_{a,i}},$$

(5)

where $P_i(t)$ [L] and $R_i(t)$ [L] are the cumulative rainfall and the cumulative runoff, respectively, at time t, both assumed uniform within the macrocell i. In addition, S_i [L] is the soil potential maximum infiltration (defined constant within each macrocell and estimated on the basis of the map of CNII shown in Fig. 2c), $I_a = \alpha c_S S$ [L] is the initial abstraction, with $\alpha < 1$ [-] introduced to represent the initial abstraction as a fraction of the maximum infiltration, and c_S [-] is a multiplicative factor accounting for uncertainty in the identification of S.

Therefore, the effective rainfall intensity p_i [L/T] at time t can be computed as follows:

$$p_i(t) = \frac{R_i(t) - R_i(t - \Delta t)}{\Delta t},$$

(6)

and Eq. (5) is applied at discrete times, according to the time step Δt.

The specific water flux produced by the hillslopes of the macrocell i can be obtained by applying mass conservation at the hillslope scale by considering the effective precipitation as inflow and runoff η as the only outflow (evapotranspiration can be neglected since the model is applied at the flood event temporal scale):

$$\frac{\eta^{(i)}(t) - \eta^{(i)}(t - \Delta t)}{\Delta t} = \frac{1}{\lambda} \left[p_i(t) - \eta^{(i)}(t - \Delta t) \right],$$

(7)

where λ [T] is the mean residence time of the linear reservoir and the left hand term is the first order approximation of the time derivative of runoff $\eta^{(i)}$. Parameters α, c_S and λ were assumed uniform through the river basin, i.e., all the macrocells share the same coefficients. On the basis of preliminary analysis α was found not to be a sensitive parameter and was set to 0.08 (which is in agreement with the values found by D'Asaro and Grillone (2012)), while c_S and λ are calibration parameters, together with the channel velocity V_c. We emphasize that this simplified hydrological model obtained as the combination of HYPERstream routing scheme and the SCS rainfall excess model is event-based since it does not include a continuous soil-moisture accounting module; however, this is enough for the purpose of this example application, mainly focused on flood events, which aim is to show how HYPERstream implements routing. As explained in Sect. 2, HYPERstream is not limited to this simplified implementation, yet effective for the purpose of flood forecasting, and can work with more sophisticated runoff generation schemes, offering a wide range of possibilities.

In order to illustrate model performance we selected two major rainfall events within the decade 1990-2000, that generated significant, yet not extreme, floods. The streamflow triggered by these rainfall events was compared with observational data at the 5 nodes described in section 3.1. The

15

two events occurred in December 1992 and February 1999, respectively. In both cases precipitation was caused by humid frontal advection from the Mediterranean Sea followed by condensation due to orographic uplift (Calenda et al., 2005). For the sake of simplicity, the spatial distribution of the

395 precipitation was not retrieved from a climatic model, but was obtained by interpolation of the measurements at the available rain gauges (18 and 32 for the events of December 1992 and February 1999, respectively) by means of Kriging with External Drift (see e.g., Goovaerts, 1997). The precipitation was interpolated separately at each time step by using the same exponential semivariogram which has been obtained by analyzing offline the available data. In particular, precipitation was first

400 calculated over a $1\,km$ resolution grid and successively aggregated at the macrocell scale, according to the resolution adopted in the simulations. We remark here that the precipitation data in input can be of any type, the reconstruction by interpolation with the kriging tool being just a simple example.

In order to test the computational efficiency of HYPERstream, model calibration was performed generating a large number (i.e., $100,000$) of model parameter sets using the Latin Hypercube Sam-

405 pling technique (McKay et al., 1979) with the following boundaries: $V_c \in [0.5, 4]$ m/s, $c_S \in [0.3, 3]$, and $\lambda \in [0.01, 1]$ d. The optimization procedure was based on the maximization of the Nash-Sutcliffe Efficiency (NSE) index (Nash and Sutcliffe, 1970) for streamflow evaluated at the outlet of the basin (i.e., Ponte Nuovo, see Fig. 3). The model was run with four spatial resolutions (i.e., 5 km, 10 km, 50 km and 150 km, see Section 3.2) with a computational time step of $\Delta t = 0.5\,h$, and calibrated on

410 the event occurred in the period 6-12 February 1999 at Ponte Nuovo (PN) station. Results in terms of optimized parameter sets, NSE index, and computational time for the entire set of $100,000$ runs are summarized in Table 2.

In all cases, the NSE index at the calibration section (PN) assumes high values, close to one, indicating a very good model fit to the observed streamflow data. Optimal parameter sets assume similar

415 values at all the scales, suggesting that the model is able to preserve geomorphological dispersion when the domain is discretized with macrocells of increasing dimension. This is verified also when a single macrocell of $150\,km$ resolution is used, though in this case the impossibility to reproduce the spatial variability of the rainfall (given that only a single macrocell is used the precipitation is considered uniform over the entire basin) resulted in an inaccurate description of inter-basin prop-

420 agation of fluxes, as emphasized by the negative values of the NSE index averaged over all nodes. Conversely, for all the other spatial resolutions, overall NSE values between 0.47 and 0.65 was obtained. Notice that all cases with the average NSE> 0.45 are with a macrocell dimension equal or smaller than the integral scale of the precipitation, which is about 36 km (E. Volpi, Modello di struttura spaziale del campo di precipitazione, unpublished technical report, available upon request). It

425 is therefore clear that the inaccuracies encountered with large macrocells are due to the inaccurate spatial description of the precipitation. Finally, the computational cost for 100,000 runs and for a single processor (Intel(R) Xeon(R) W5580 @ 3.20 GHz core), the code being written in Fortran 90, is shown to increase from a few seconds in the case of one single macrocell to about 10 minutes

for the finer resolution (1 km, corresponding to 476 macrocells). We emphasize that the computational efforts can be reduced considerably by implementing parallel computing techniques, to which HYPERstream is particularly suited thanks to its inherently parallel formulation (see also Section 2).

Model validation was carried out by means of a combined multi-site, multi-event approach, and was coupled with a Monte Carlo based uncertainty analysis performed on a subset of parameter combinations sampled during calibration at PN with the 1999 flood event as observational data. This subset was identified according to a model efficiency rejection criterion that classifies as behavioral all sets of parameters with a NSE index greater than zero, resulting in 21 501 parameters sets and model realizations. Successively, the 95% uncertainty bands associated with the retained simulations were evaluated using the standard likelihood weighted procedure proposed by Freer et al. (1996). Results obtained for the 10 km spatial resolution configuration are presented in Fig. 6, which shows 95% prediction uncertainty bands and observed streamflow at the 5 nodes shown in Fig. 3. Simulated hydrographs obtained adopting the optimal parameter set reported in Table 2 are also shown with a continuous black line. Subplots 6a-e show uncertainty bands for the February 1999 event (the calibration event) considering all the gauging stations including PN, which was the only used in calibration. Other indicators of goodness are P- and R-factors (see e.g., Abbaspour et al., 2009), which are defined as the percentage of data bracketed by the confidence band, and the ratio between the average width of the band and the standard deviation of observations, respectively. Computed water discharge at all nodes provided high P-factor values (96% for SL and PR, and 100% for all the others), and moderate R-factor values (2.02, 2.36, 1.52, 3.67, and 3.29 for PN, PF, SL, PR, and PB, respectively). The somewhat suboptimal performance with respect to the R-factor is in part due to the decision of considering behavioral all the models with NSE> 0, instead of the typical choice of setting the threshold at NSE$= 0.5$, with the consequent reduction of the uncertainty band thus of the R-factor. Visual inspection of Fig. 6 and the above performance factors indicate that the model is able to encompass most of the observed discharges, while retaining reasonable uncertainty band amplitudes. The same analysis was performed also for the event occurred between 4 and 7 December 1992 (multi-site, multi-event validation). Results are presented in subplots 6f-i, which suggest reasonable model prediction capability (P-factor equal to 100%, 83%, 59%, 100%, and R-factor equal to 1.85, 1.76, 1.50, and 2.37, for PN, PF, SL, and PB, respectively; we note that no water discharge data were available at PR during this event), although a general tendency to underestimate the flood volume is evident. This is likely due to inherent differences between precipitation conditions (e.g., intensity, spatial distribution) during the two events and in the preceding days, which reflect into different initial soil moisture conditions that cannot be fully captured with the simple event-based SCS-CN model used here.

17

4 Conclusions

465 This work presents an innovative, multi-scale streamflow routing method based on the travel time approach. The principal aim is to develop a simple, parsimonious and computationally efficient method for modeling streamflow (and particularly floods) in large basins. The model, coined as HYPERstream, aims at correctly reproduce the relevant horizontal hydrological fluxes across the scales of interest, from a single catchment to the whole continent. The method is based on the WFIUH

470 theory applied to a hybrid raster-vector data structure, that allows to derive localized information on travel times and flow characteristics without the need of narrowing the resolution of the computational grid adopted for the study area. The relevant features of the model are illustrated through the modeling of two flood events in the Upper Tiber river basin (central Italy), with 4 different domain discretizations, i.e., different dimensions of macrocells.

475   The main results of the present work can be summarized as follows.

– HYPERstream employs a strategy for modeling cell-scale runoff dispersivity such that the simulation of horizontal hydrological fluxes is independent from the grid size, which in turn is function of the resolution of the atmospheric model or the integral scale of observed precipitation (in case ground-based rainfall measurements are used as in the example application

480   provided here). In particular, the contribution of the geomorphological dispersion is kept invariant at all spatial scales, since in our scheme river network response is derived from the morphological information embedded in the available DEM. This "perfect upscaling" characteristic of HYPERstream is particularly important in all cases when the catchment response needs to be accurately represented, e.g. when dealing with extreme events like floods and

485   inundations.

– The above "perfect upscaling" characteristic allows adopting large cells, making the model suitable to large-scale models, up to the continental scale. The overall response function of the river networks will anyway be preserved, no matter the discretization.

– Computational efficiency is another relevant feature of the proposed approach. Efficiency

490   stems from the fact that the demanding calculation of the width functions is a pre-processing, one-time effort. Furthermore, the model is prone to parallelization, stemming from the linearity of routing and independency of the runoff generation module adopted at the cell scale. These features make HYPERstream an appealing tool for uncertainty assessment of the predictions, and for simulations conducted in a Monte Carlo framework.

495 – The routing component of the model (including hillslope routing) depends on two parameters, with the additional parameters inherited from the conceptual model of runoff generation adopted at the hillslope scale. While in principle no limitations are posed to the latter conceptualization, we are in favor of a pragmatic "downward" approach, which limits the total number

18

500   of parameters, to reduce uncertainty and overparameterization. Parsimony is important for a
meaningful and reliable parameter estimation procedure and uncertainty analysis.

We believe that all of the above characteristics make of HYPERstream an appealing routing tool to
be implemented in LHMs, particularly suitable for climate change impact studies where the accuracy
of the streamflow routing may be significantly affected by the spatial resolution adopted.

References

Abbaspour, K. C., Faramarzi, M., Ghasemi, S. S., and Yang, H.: Assessing the impact of climate change on water resources in Iran, Water Resour. Res., 45, W10 434, doi:10.1029/2008WR007615, 2009.

Archfield, S. A., Clark, M., Arheimer, B., Hay, L. E., McMillan, H., Kiang, J. E., Seibert, J., Hakala, K., Bock, A., Wagener, T., Farmer, W. H., Andréassian, V., Attinger, S., Viglione, A., Knight, R., Markstrom, S., and Over, T.: Accelerating advances in continental domain hydrologic modeling, Water Resources Research, p. in press, doi:10.1002/2015WR017498, 2015.

Arnell, N. W.: A simple water balance model for the simulation of streamflow over a large geographic domain, J. Hydrol., 217, 314–335, doi:10.1016/S0022-1694(99)00023-2, 1999.

Bellin, A., Majone, B., Cainelli, O., Alberici, D., and Villa, F.: A continuous coupled hydrological and water resources management model, Environmental Modelling and Software, 75, 176–192, doi:10.1016/j.envsoft.2015.10.013, 2016.

Botter, G. and Rinaldo, A.: Scale effect on geomorphologic and kinematic dispersion, Water Resour. Res., 39, SWC61–SWC610, doi:10.1029/2003WR002154, 2003.

Calenda, G., Gorgucci, E., Napolitano, F., Novella, A., and Volpi, E.: Multifractal analysis of radar rainfall fields over the area of Rome, Adv. Geosci., 2, 293–299, doi:10.5194/adgeo-2-293-2005, 2005.

Clark, M. P., Fan, Y., Lawrence, D. M., Adam, J. C., Bolster, D., Gochis, D. J., Hooper, R. P., Kumar, M., Leung, L. R., Mackay, D. S., Maxwell, R. M., Shen, C., Swenson, S. C., and Zeng, X.: Improving the representation of hydrologic processes in Earth System Models, Water Resour. Res., pp. n/a–n/a, doi:10.1002/2015WR017096, 2015.

D'Asaro, F. and Grillone, G.: Empirical Investigation of Curve Number Method Parameters in the Mediterranean Area, J. Hydrol. Eng., 17, 1141–1152, doi:10.1061/(ASCE)HE.1943-5584.0000570, 2012.

De Barros, F. P. J. and Rubin, Y.: Modelling of block-scale macrodispersion as a random function, J. Fluid Mech., 676, 514–545, doi:10.1017/jfm.2011.65, 2011.

De Paiva, R. C. D., Buarque, D. C., Collischonn, W., Bonnet, M. P., Frappart, F., Calmant, S., and Bulhões Mendes, C. A.: Large-scale hydrologic and hydrodynamic modeling of the Amazon River basin, Water Resour. Res., 49, 1226–1243, doi:10.1002/wrcr.20067, 2013.

Di Lazzaro, M.: Regional analysis of storm hydrographs in the Rescaled Width Function framework, J. Hydrol., 373, 352–365, doi:10.1016/j.jhydrol.2009.04.027, 2009.

Di Lazzaro, M. and Volpi, E.: Effects of hillslope dynamics and network geometry on the scaling properties of the hydrologic response, Adv. Water Resour., 34, 1496–1507, doi:10.1016/j.advwatres.2011.07.012, 2011.

D'Odorico, P. and Rigon, R.: Hillslope and channel contributions to the hydrologic response, Water Resour. Res., 39, SWC11–SWC19, doi:10.1029/2002WR001708, 2003.

Döll, P., Kaspar, F., and Lehner, B.: A global hydrological model for deriving water availability indicators: Model tuning and validation, J. Hydrol., 270, 105–134, doi:10.1016/S0022-1694(02)00283-4, 2003.

ESRI: ArcGIS Desktop: Release 10, Environmental Systems Research Institute, Redlands, CA, USA, http://www.esri.com/software/arcgis/arcgis-for-desktop, 2011.

Freer, J., Beven, K., and Ambroise, B.: Bayesian estimation of uncertainty in runoff prediction and the value of data: An application of the GLUE approach, Water Resour. Res., 32, 2161–2173, doi:10.1029/95WR03723, 1996.

20

550 Giannoni, F., Roth, G., and Rudari, R.: A procedure for drainage network identification from geomorphology and its application to the prediction of the hydrologic response, Adv. Water Resour., 28, 567–581, doi:10.1016/j.advwatres.2004.11.013, 2005.

Gong, L., Widén-Nilsson, E., Halldin, S., and Xu, C. Y.: Large-scale runoff routing with an aggregated network-response function, J. Hydrol., 368, 237–250, doi:10.1016/j.jhydrol.2009.02.007, 2009.

555 Gong, L., Halldin, S., and Xu, C. Y.: Global-scale river routing-an efficient time-delay algorithm based on HydroSHEDS high-resolution hydrography, Hydrol. Process., 25, 1114–1128, doi:10.1002/hyp.7795, 2011.

Goovaerts, P.: Geostatistics for natural resources evaluation, University Press, Oxford, USA, 1997.

Gupta, V. K. and Mesa, O. J.: Runoff generation and hydrologic response via channel network geomorphology - recent progress and open problems, J. Hydrol., 102, 3–28, doi:10.1016/0022-1694(88)90089-3, 1988.

560 Gupta, V. K., Waymire, E., and Rodríguez-Iturbe, I.: On Scales, Gravity and Network Structure in Basin Runoff, in: Scale Problems in Hydrology, edited by Gupta, V. K., Rodríguez-Iturbe, I., and Wood, E. F., vol. 6 of *Water Science and Technology Library*, pp. 159–184, Springer Netherlands, doi:10.1007/978-94-009-4678-1_8, 1986.

Haddeland, I., Clark, D. B., Franssen, W., Ludwig, F., Voß, F., Arnell, N. W., Bertrand, N., Best, M., Folwell, S., Gerten, D., Gomes, S., Gosling, S. N., Hagemann, S., Hanasaki, N., Harding, R., Heinke, J., Kabat, P., Koirala, S., Oki, T., Polcher, J., Stacke, T., Viterbo, P., Weedon, G. P., and Yeh, P.: Multimodel estimate of the global terrestrial water balance: Setup and first results, J. Hydrometeorol., 12, 869–884, doi:10.1175/2011JHM1324.1, 2011.

Hallema, D. W. and Moussa, R.: A model for distributed GIUH-based flow routing on natural and anthropogenic
570 hillslopes, Hydrological Processes, 28, 4877–4895, doi:10.1002/hyp.9984, 2014.

Hallema, D. W., Moussa, R., Andrieux, P., and Voltz, M.: Parameterization and multi-criteria calibration of a distributed storm flow model applied to a Mediterranean agricultural catchment, Hydrol. Process., 27, 1379–1398, doi:10.1002/hyp.9268, 2013.

Hanasaki, N., Kanae, S., Oki, T., Masuda, K., Motoya, K., Shirakawa, N., Shen, Y., and Tanaka, K.: An integrated model for the assessment of global water resources - Part 1: Model description and input meteorological forcing, Hydrol. Earth Syst. Sci., 12, 1007–1025, doi:10.5194/hess-12-1007-2008, 2008a.

Hanasaki, N., Kanae, S., Oki, T., Masuda, K., Motoya, K., Shirakawa, N., Shen, Y., and Tanaka, K.: An integrated model for the assessment of global water resources - Part 2: Applications and assessments, Hydrol. Earth Syst. Sci., 12, 1027–1037, doi:10.5194/hess-12-1027-2008, 2008b.

580 Kavvas, M. L., Kure, S., Chen, Z. Q., Ohara, N., and Jang, S.: WEHY-HCM for Modeling Interactive Atmospheric-Hydrologic Processes at Watershed Scale. I: Model Description, J. Hydrol. Eng., 18, 1262–1271, doi:10.1061/(ASCE)HE.1943-5584.0000724, 2013.

Lehner, B. and Grill, G.: Global river hydrography and network routing: Baseline data and new approaches to study the world's large river systems, Hydrol. Process., 27, 2171–2186, doi:10.1002/hyp.9740, 2013.

585 Lehner, B., Verdin, K., and Jarvis, A.: HydroSHEDS Technical Documentation, Version 1.0, Tech. rep., World Wildlife Fund US, Washington, DC, available at http://hydrosheds.cr.usgs.gov, 2006.

Lehner, B., Verdin, K., and Jarvis, A.: New global hydrography derived from spaceborne elevation data, EOS, Trans. Am. Geophys. Union, 89, 93–94, doi:10.1029/2008EO100001, 2008.

Liang, X., Lettenmaier, D. P., Wood, E. F., and Burges, S. J.: A simple hydrologically based model of land
surface water and energy fluxes for general circulation models, J. Geophys. Res.-Atmos, 99, 14 415–14 428,
doi:10.1029/94JD00483, 1994.

Manabe, S.: Climate and the ocean circulation: 1. The atmospheric circulation and the hydrology of the Earth's
surface, Mon. Weather Rev., 97, 739–805, 1969.

Manfreda, S., Nardi, F., Samela, C., Grimaldi, S., Taramasso, A. C., Roth, G., and Sole, A.: Investigation
on the use of geomorphic approaches for the delineation of flood prone areas, J. Hydrol., 517, 863–876,
doi:10.1016/j.jhydrol.2014.06.009, 2014.

McKay, M. D., Beckman, R. J., and Conover, W. J.: A Comparison of Three Methods for Selecting Val-
ues of Input Variables in the Analysis of Output from a Computer Code, Technometrics, 21, 239–245,
doi:10.2307/1268522, 1979.

Mesa, O. J. and Mifflin, E. R.: On the Relative Role of Hillslope and Network Geometry in Hydrologic Re-
sponse, in: Scale Problems in Hydrology, edited by Gupta, V. K., Rodríguez-Iturbe, I., and Wood, E. F., vol. 6
of *Water Science and Technology Library*, pp. 1–17, Springer Netherlands, doi:10.1007/978-94-009-4678-
1_1, 1986.

Milly, P. C. D. and Shmakin, A. B.: Global modeling of land water and energy balances.
Part I: The land dynamics (LaD) model, J. Hydrometeorol., 3, 283–299, doi:10.1175/1525-
7541(2002)003<0283:GMOLWA>2.0.CO;2, 2002.

Montgomery, D. R. and Foufoula-Georgiou, E.: Channel network source representation using digital elevation
models, Water Resour. Res., 37, 53–71, doi:10.1080/02626669209492561, 1992.

Moussa, R.: Geomorphological transfer function calculated from digital elevation models for distributed hydro-
logical modelling, Hydrol. Process., 11, 429–449, doi:10.1002/(SICI)1099-1085(199704)11:5<429::AID-
HYP471>3.0.CO;2-J, 1997.

Naden, P. S.: Spatial variability in flood estimation for large catchments: the exploitation of channel network
structure, 37, 53–71, doi:10.1080/02626669209492561, 1992.

Nash, J. E. and Sutcliffe, J. V.: River flow forecasting through conceptual models part I. A discussion of princi-
ples, J. Hydrol., 10, 282–290, doi:10.1016/0022-1694(70)90255-6, 1970.

Nazemi, A. and Wheater, H. S.: On inclusion of water resource management in Earth system models -
Part 1: Problem definition and representation of water demand, Hydrol. Earth Syst. Sci., 19, 33–61,
doi:10.5194/hess-19-33-2015, 2015.

Nicótina, L., Alessi Celegon, E., Rinaldo, A., and Marani, M.: On the impact of rainfall patterns on the hydro-
logic response, Water Resour. Res., 44, doi:10.1029/2007WR006654, 2008.

Niu, G. Y., Yang, Z. L., Mitchell, K. E., Chen, F., Ek, M. B., Barlage, M., Kumar, A., Manning, K., Niyogi, D.,
Rosero, E., Tewari, M., and Xia, Y.: The community Noah land surface model with multiparameterization
options (Noah-MP): 1. Model description and evaluation with local-scale measurements, J. Geophys. Res.-
Atmos., 116, doi:10.1029/2010JD015139, 2011.

O'Callaghan, J. F. and Mark, D. M.: The extraction of drainage networks from digital elevation data., Comput.
Vision Graph., 28, 323–344, 1984.

Oleson, K., Lawrence, D. M., Bonan, G. B., Drewniak, B., Huang, M., Koven, C. D., Levis, S., Li, F., Ri-
ley, W. J., Subin, Z. M., Swenson, S., Thornton, P. E., Bozbiyik, A., Fisher, R., Heald, C. L., Kluzek, E.,

Lamarque, J. F., Lawrence, P. J., Leung, L. R., Lipscomb, W., Muszala, S. P., Ricciuto, D. M., Sacks, W. J.,

630 Sun, Y., Tang, J., and Yang, Z. L.: Technical description of version 4.5 of the Community Land Model (CLM). NCAR Technical Note NCAR/TN-503+STR, Tech. rep., National Center for Atmospheric Research, doi:10.5065/D6RR1W7M, 2013.

Pilgrim, D. H.: Travel times and nonlinearity of flood runoff from tracer measurements on a small watershed, Water Resour. Res., 12, 487–496, doi:10.1029/WR012i003p00487, 1976.

635 Pilgrim, D. H.: Isochrones of travel time and distribution of flood storage from a tracer study on a small watershed, Water Resour. Res., 13, 587–595, doi:10.1029/WR013i003p00587, 1977.

Prentice, I. C., Liang, X., Medlyn, B. E., and Wang, Y. P.: Reliable, robust and realistic: the three R's of next-generation land-surface modelling, Atmospheric Chemistry and Physics, 15, 5987–6005, doi:10.5194/acp-15-5987-2015, 2015.

640 Rigon, R., Bancheri, M., Formetta, G., and de Lavenne, A.: The geomorphic unit hydrograph from a historical-critical perspective, Earth Surf. Proc. Land., doi:10.1002/esp.3855, early View, 2015.

Rinaldo, A., Marani, A., and Rigon, R.: Geomorphological dispersion, Water Resour. Res., 27, 513–525, doi:10.1029/90WR02501, 1991.

Rinaldo, A., Vogel, G. K., Rigon, R., and Rodriguez-Iturbe, I.: Can One Gauge the Shape of a Basin?, Water

645 Resour. Res., 31, 1119–1127, doi:10.1029/94WR03290, 1995.

Rinaldo, A., Botter, G., Bertuzzo, E., Uccelli, A., Settin, T., and Marani, M.: Transport at basin scales: 1. Theoretical framework, Hydrol. Earth Syst. Sci., 10, 19–29, doi:10.5194/hess-10-19-2006, 2006.

Rodríguez-Iturbe, I. and Rinaldo, A.: Fractal river basins: Chance and self-organization, Cambridge University Press, Cambridge, UK, 1997.

650 Rubin, Y., Sun, A., Maxwell, R., and Bellin, A.: The concept of block-effective macrodispersivity and a unified approach for grid-scale- and plume-scale-dependent transport, J. Fluid Mech., 395, 161–180, doi:10.1017/S0022112099005868, 1999.

Samaniego, L., Kumar, R., and Attinger, S.: Multiscale parameter regionalization of a grid-based hydrologic model at the mesoscale, Water Resour. Res., 46, doi:10.1029/2008WR007327, 2010.

655 Sapriza-Azuri, G., Jódar, J., Navarro, V., Slooten, L. J., Carrera, J., and Gupta, H. V.: Impacts of rainfall spatial variability on hydrogeological response, Water Resour. Res., 51, 1300–1314, doi:10.1002/2014WR016168, 2015.

Sivapalan, M.: Process complexity at hillslope scale, process simplicity at the watershed scale: is there a connection?, Hydrol. Process., 17, 1037–1041, doi:10.1002/hyp.5109, 2003.

660 Tarboton, D. G., Bras, R. L., and Rodrìguez-Iturbe, I.: On the extraction of channel networks from digital elevation data, Hydrol. Process., 5, 81–100, doi:10.1002/hyp.3360050107, 1991.

U.S. Soil Conservation Service: SCS National Engineering Handbook, vol. Hydrology, Section 4, U.S. Department of Agriculture, Washington D.C., 1964.

Van Beek, L. P. H., Wada, Y., and Bierkens, M. F. P.: Global monthly water stress: 1. Water balance and water

665 availability, Water Resour. Res., 47, doi:10.1029/2010WR009791, 2011.

van der Knijff, J. M., Younis, J., and de Roo, A. P. J.: LISFLOOD: A GIS-based distributed model for river basin scale water balance and flood simulation, Int. J. Geogr. Inf. Sci., 24, 189–212, doi:10.1080/13658810802549154, 2010.

Van Der Tak, L. D. and Bras, R. L.: Incorporating hillslope effects into the geomorphologic instantaneous unit hydrograph, Water Resour. Res., 26, 2393–2400, doi:10.1029/90WR00862, 1990.

Verzano, K., Bärlund, I., Flörke, M., Lehner, B., Kynast, E., Voß, F., and Alcamo, J.: Modeling variable river flow velocity on continental scale: Current situation and climate change impacts in Europe, J. Hydrol., 424–425, 238–251, doi:10.1016/j.jhydrol.2012.01.005, 2012.

Volpi, E., Di Lazzaro, M., and Fiori, A.: A simplified framework for assessing the impact of rainfall spatial variability on the hydrologic response, Adv. Water Resour., 46, 1–10, doi:10.1016/j.advwatres.2012.04.011, 2012.

Vörösmarty, C. J., Federer, C. A., and Schloss, A. L.: Potential evaporation functions compared on US watersheds: Possible implications for global-scale water balance and terrestrial ecosystem modeling, J. Hydrol., 207, 147–169, doi:10.1016/S0022-1694(98)00109-7, 1998.

Wen, Z., Liang, X., and Yang, S.: A new multiscale routing framework and its evaluation for land surface modeling applications, Water Resour. Res., 48, doi:10.1029/2011WR011337, 2012.

Whiteaker, T. L., Maidment, D. R., Goodall, J. L., and Takamatsu, M.: Integrating arc hydro features with a schematic network, Trans. GIS, 10, 219–237, doi:10.1111/j.1467-9671.2006.00254.x, 2006.

Widén-Nilsson, E., Halldin, S., and Xu, C. y.: Global water-balance modelling with WASMOD-M: Parameter estimation and regionalisation, J. Hydrol., 340, 105–118, doi:10.1016/j.jhydrol.2007.04.002, 2007.

Wood, E. F., Roundy, J. K., Troy, T. J., van Beek, L. P. H., Bierkens, M. F. P., Blyth, E., de Roo, A., Doell, P., Ek, M., Famiglietti, J., Gochis, D., van de Giesen, N., Houser, P., Jaffe, P. R., Kollet, S., Lehner, B., Lettenmaier, D. P., Peters-Lidard, C., Sivapalan, M., Sheffield, J., Wade, A., and Whitehead, P.: Hyperresolution global land surface modeling: Meeting a grand challenge for monitoring Earth's terrestrial water, Water Resour. Res., 47, doi:10.1029/2010WR010090, 2011.

Yamazaki, D., Kanae, S., Kim, H., and Oki, T.: A physically based description of floodplain inundation dynamics in a global river routing model, Water Resour. Res., 47, doi:10.1029/2010WR009726, 2011.
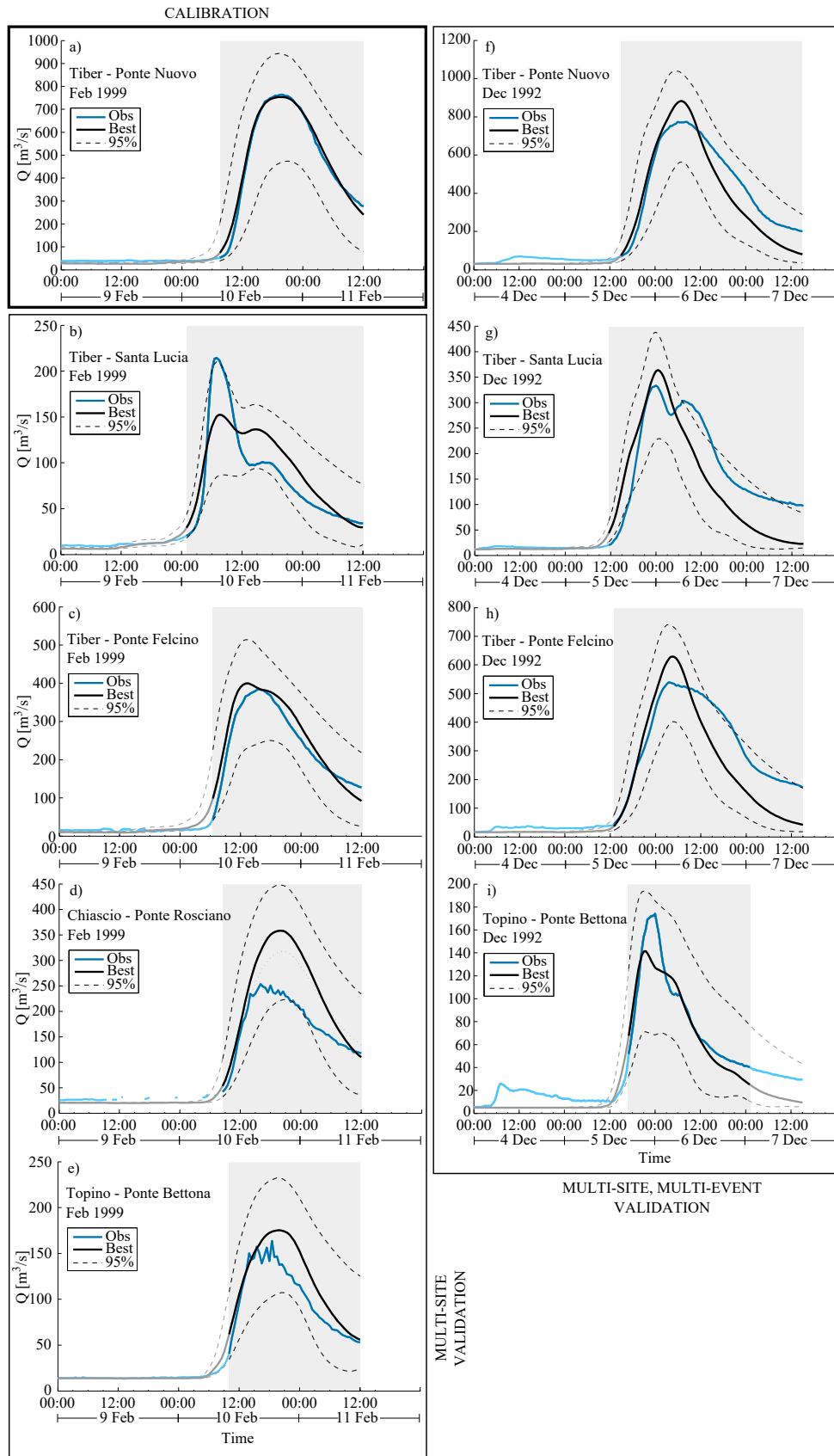
Figure 6. Comparison between 95% confidence band, water discharge simulated with the optimal parameter set and observed at all the gauging stations and events: subplots a-e 6-12 February 1999, and subplots e-i 4-7 December 1992. Shaded areas identify the period considered in the evaluation of P- and R-factors. Model

Table 1. Main geomorphic characteristics of the inter-basin drainage areas within the Upper Tiber river basin (CV: Coefficient of Variation).

Basin	ID	Area [km^2]	Slope [m/m]	Channel Length Statistics			
				Max [km]	Mean [m]	Variance [m^2]	CV [m/m]
Tiber at Santa Lucia	SL	932	0.009	66.1	32482	2.03E+08	0.44
Tiber at Ponte Felcino	PF	2032	0.005	112.6	60201	6.97E+08	0.44
Topino at Ponte Bettona	PB	1180	0.009	65.1	37495	2.41E+08	0.41
Chiascio at Ponte Rosciano	PR	1909	0.007	92.9	48477	4.74E+08	0.45
Tiber at Ponte Nuovo	PN	4116	0.005	139.6	67410	8.84E+08	0.44

Table 2. Optimal model parameters, calibrated at Ponte Nuovo station (event February 1999), Nash-Sutcliffe efficiency indexes for Ponte Nuovo and all nodes, and computational time cost (for 100,000 runs) resulting from the calibration procedure, for different spatial scale resolutions (size of the macrocell).

Spatial scale	n. macrocells	V_c [m/s]	c_s [-]	λ [d]	NSE [-] (PN)	NSE [-] (all nodes)	comp. time [min]
5 km	476	2.28	1.19	0.34	0.99	0.64	10.2
10 km	126	2.44	1.12	0.35	0.99	0.47	3.00
50 km	6	2.39	1.07	0.31	0.98	0.65	0.44
150 km	1	2.47	0.83	0.29	0.94	-0.59	0.22